13th International Symposium on Turbulence and Shear Flow Phenomena (TSFP13)
Montreal, Canada, June 25–28, 2024

ON THE DYNAMICS OF INSTANTANEOUS WALL-NORMAL INTEGRALS

Perry L. Johnson
Department of Mechanical & Aerospace Engineering
University of California, Irvine
Irvine, CA, 92697
perry.johnson@uci.edu

Tanner Ragan
Department of Mechanical & Aerospace Engineering
University of California, Irvine
Irvine, CA, 92697
ragant@uci.edu

ABSTRACT

Large (and very-large) scale motions produce much of the turbulent kinetic energy and Reynolds shear stress in wall-bounded flows. Their streamwise extent can exceed the thickness of the wall layer, while their spanwise and wall-normal extents are typically comparable to it. As such, even when instantaneous velocity fields are integrated in the wall-normal direction across the entire wall layer, the resulting two-dimensional representation still contains significant turbulent structure. The wall-normal integration of the Reynolds-averaged equation has long been used for low-cost models for turbulent boundary layers, i.e., integral methods. By comparison, instantaneous wall-normal integrals are largely unexplored, despite their potential to efficiently encapsulate large-scale dynamics. In this work, dynamical equations for instantaneous wall-normal integrals are derived directly from the Navier-Stokes equation. Data from direct numerical simulations of canonical wall-bounded flows are used to analyze the dynamics of instantaneous integrals. The results show that instantaneous wall-normal integrals can capture a significant majority of the turbulent shear stresses from large-scale motions, providing a potential avenue for constructing predictive models.

INTRODUCTION

The development and use of integral-based tools to analyze and model boundary layers stretches back more than a century, beginning with laminar boundary layers (von Kármán, 1921; Pohlhausen, 1921; Thwaites, 1949) and then extending to turbulent flows using wall-normal integrals of the Reynolds-averaged Navier-Stokes (RANS) equation (Kline *et al.*, 1968). The rise of digital computers enabled the solution of fully three-dimensional partial differential equations; first using the RANS equations, then later using scale-resolving approaches such as Direct Numerical Simulations (DNS) and Large-Eddy Simulations (LES), including both hybrid RANS/LES and wall-modeling approaches. DNS, of course, remains too costly for the high Reynolds numbers typically involved in most applications of interest. Meanwhile, cheaper approaches such as wall-modeled LES still carry a very high cost at application-relevant Reynolds numbers (Yang & Griffin, 2021; Goc *et al.*, 2020), even with a coarse resolution of five to ten grid points across the boundary layer.

The strong influence of turbulent motions with streamwise extent comparable to (and exceeding) the boundary layer thickness, channel half-height, or pipe radius raises intriguing modeling challenges and opportunities (Jimenez, 1998; Kim & Adrian, 1999; Guala *et al.*, 2006; Balakumar & Adrian, 2007; Hutchins & Marusic, 2007; Monty *et al.*, 2009). These large scale motions (LSMs), superstructures, and very-large scale motions (VLSMs) have substantial wall-normal extent (see, e.g., Fig. 13 of Lee *et al.* (2017)), are responsible for a significant portion of the turbulent kinetic energy (TKE) and Reynolds stress throughout most of the boundary layer, and are keenly sensitive to pressure gradients (Harun *et al.*, 2013). The main challenge for developing models for wall-bounded turbulence based on (V)LSMs is how to develop an efficient framework that is directly based on first principles, that is, the Navier-Stokes equation.

In this work, the use of instantaneous wall-normal integrals (i.e., an 'LES' version of classical RANS-based integral methods) is proposed and investigated as one possible way to address this challenge. The feasibility of such an approach is illustrated in Figure 1 using turbulent channel flow data. Even after integrating the instantaneous velocity field across the channel half-height, the dominant features of the turbulent fluctuations remain. The goal of this work is to derive the dynamical equations for instantaneous integrals from the Navier-Stokes equation and to study unclosed terms which arise, providing quantitative analysis of the observations in Figure 1.

THEORY

To begin the investigation, the dynamical equations for instantaneous wall-normal integrals are derived for a half-channel flow with a no-slip, no-penetration boundary condition at the bottom wall and a no-penetration, no-vorticity condition at the top wall. While integral formulations are commonly deployed for spatially-developing boundary layers, the half-channel allows for two directions of homogeneity, making it a useful surrogate flow to begin studying the dynamics

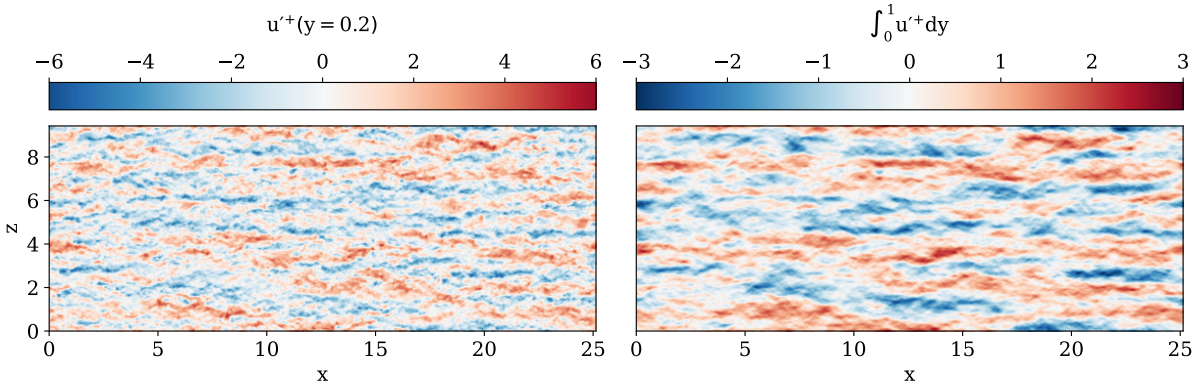

Figure 1. Comparison of the instantaneous streamwise velocity on a wall-parallel plane at $y = 0.2$ (left) with the wall-normal integrated velocity at the same instant in time (right). Data from the $Re_t = 1000$ channel flow JHTDB dataset.

of wall-normal integrals. The following formulation for half-channel flows can be extended to external boundary layer flows using the velocity defect compared to an inviscid or potential flow solution.

In this work, the equations of motion are non-dimensionalized using the friction velocity (u_t) and the half-channel height (h). The wall-normal y coordinate is treated separately from the streamwise and spanwise coordinates, so the index range is $i = 1,2$ and implied summation is only over these two indices. Thus, the wall-parallel coordinates are $x_1 = x$ and $x_2 = z$ for the streamwise and spanwise directions, respectively. Likewise the streamwise and spanwise velocity components are $u_1 = u$ and $u_2 = w$, respectively, and the wall-normal velocity is v. The conservation of mass for incompressible flows is

$$\frac{\partial u_i}{\partial x_i} + \frac{\partial v}{\partial y} = 0. \tag{1}$$

and wall-parallel momentum conservation is

$$\frac{\partial u_i}{\partial t} + \frac{\partial (u_i u_j)}{\partial x_j} + \frac{\partial (u_i v)}{\partial y} = -\frac{\partial p}{\partial x_i} + \frac{1}{Re_t}\left(\frac{\partial^2 u_i}{\partial x_j \partial x_j} + \frac{\partial^2 u_i}{\partial y^2}\right) + d_{i1}. \tag{2}$$

Finally, the conservation of wall-normal momentum is

$$\frac{\partial v}{\partial t} + \frac{\partial (v u_j)}{\partial x_j} + \frac{\partial (v^2)}{\partial y} = -\frac{\partial p}{\partial y} + \frac{1}{Re_t}\left(\frac{\partial^2 v}{\partial x_j \partial x_j} + \frac{\partial^2 v}{\partial y^2}\right). \tag{3}$$

Here, the p is the pressure (divided by density).

Wall-normal integrals are defined for the zeroth and first moments of any variable f as,

$$\langle f \rangle_0 = \int_0^1 f\, dy; \qquad \langle f \rangle_1 = \int_0^1 2y f\, dy. \tag{4}$$

The zeroth and first moments of the mass conservation equation yield,

$$\frac{\partial \langle u_i \rangle_0}{\partial x_i} = 0; \qquad \frac{\partial \langle u_i \rangle_1}{\partial x_i} = 2\langle v \rangle_0. \tag{5}$$

That is, the zeroth wall-normal moment of the instantaneous wall-parallel velocity is divergence free (in two dimensions) and the divergence of the first moment is proportional to the zeroth moment of the wall-normal velocity. The zeroth moment of the conservation equation for streamwise and spanwise momentum are

$$\frac{\partial \langle u_i \rangle_0}{\partial t} + \frac{\partial \langle u_i u_j \rangle_0}{\partial x_j} = -\frac{\partial \langle p \rangle_0}{\partial x_i} + \frac{1}{Re_t}\frac{\partial^2 \langle u_i \rangle_0}{\partial x_j \partial x_j} + t_i + d_{i1}; \tag{6}$$

where t_i is the instantaneous wall shear stress vector. The corresponding equation for the first moment is

$$\frac{\partial \langle u_i \rangle_1}{\partial t} + \frac{\partial \langle u_i u_j \rangle_1}{\partial x_j} = 2\langle u_i v \rangle_0 - \frac{\partial \langle p \rangle_1}{\partial x_i} + \frac{1}{Re_t}\frac{\partial^2 \langle u_i \rangle_1}{\partial x_j \partial x_j} - \frac{2U_i}{Re_t} + d_{i1} \tag{7}$$

where $U_i = u_i|_{z=1}$ is the instantaneous wall-parallel velocity at the top boundary. The wall shear stress (t_i) and top velocity (U_i) are unclosed, as are the quadratic moments: $\langle u_i u_j \rangle_0$, $\langle u_i u_j \rangle_1$, and $\langle u_i v \rangle_0$. The two pressure moments may be found by solving elliptic equations formed from the divergence of equations (6) and (7), together with equation (5). The zeroth moment of pressure is

$$\frac{\partial^2 \langle p \rangle_0}{\partial x_i \partial x_i} = \frac{\partial^2 \langle u_i u_j \rangle_0}{\partial x_i \partial x_j} - \frac{\partial t_i}{\partial x_i}. \tag{8}$$

This pressure moment enforces the two-dimensional divergence free condition in Equation (5). Finally, the first moment of pressure is

$$\frac{\partial^2 \langle p \rangle_1}{\partial x_i \partial x_i} = 2\,p|_{y=0}^{y=1} + 4\frac{\partial \langle u_i v \rangle_0}{\partial x_i} - \frac{\partial^2 \langle u_i u_j \rangle_1}{\partial x_i \partial x_j}. \tag{9}$$

The statistics and dynamics of instantaneous wall-normal integrals are explored in this work using these equations with DNS data, with particular attention to unclosed terms that would need to be approximated in terms of the solution fields $\langle u_i \rangle_0$ and $\langle u_i \rangle_1$ to form a closed model.

SIMULATION DATASETS

Direct numerical simulations (DNS) of half-channel flow are performed at $Re_t = 180$ and $Re_t = 395$ (based on the height of the half-channel) to provide data for the present investigation. The incompressible Navier-Stokes equation is solved on a staggered Cartesian grid using 2nd-order central differencing and an explicit 3rd-order Runge-Kutta scheme for time advancement (Lozano-Durán *et al.*, 2018). To facilitate

statistical comparisons between half-channel and full-channel flows, two full-channel simulations are also performed using no-slip conditions at both top and bottom walls with $Re_t = 180$ and 395 (based on the half-height of the full channel). Finally, data from the $Re_t = 1000$ channel flow simulation from the Johns Hopkins Turbulence Databases (JHTDB) are also used (Graham *et al.*, 2016). The list of flow cases is summarized in Table 1 along with the plot style for each case in the figures.

Table 1. List of DNS databases analyzed in this paper.

Case	Configuration	Re_t	Legend
180hc	half-channel	180	- - - - - -
395hc	half-channel	395	- - - - - -
180fc	full-channel	180	————
395fc	full-channel	395	————
1000fc	full-channel	1000	————

For all cases, the streamwise and spanwise lengths are $L_x = 8\pi$ and $L_z = 3\pi$, respectively. To maintain appropriate accuracy for the second-order staggered finite-difference DNS cases, the constraint for the grid spacing based on inner units for the streamwise and spanwise directions are $\Delta x^+ \approx 7.0$ and $\Delta z^+ \approx 6.0$, respectively. Additionally, the constraints for the wall-normal grid spacing at the wall and at the center are $\Delta y_w^+ \approx 0.5$ and $\Delta y_{max}^+ \approx 6.0$, respectively. The sufficiency of this mesh resolution was validated by accurately matching the one point statistics between the simulation data and Moser *et al.* (1999). Specifically, the mean velocity and Reynolds stress component profiles were sufficiently matched (not shown).

RESOLUTION ANALYSIS

Qualitatively, Figure 1 demonstrates how salient turbulence structures are resolved even after applying a wall-normal integral across the entire wall layer. In this section, the ability of the two-dimensional integral field, $\langle f \rangle_{0;1}$, to resolve turbulent dynamics is analyzed quantitatively. The wall shear stress vector, τ_i, provides a local sink for the zeroth moment of momentum equation, Eq. (6). This wall shear stress is completely unresolved and requires closure modeling, as is typical for integral approaches. However, the local sink of the first moment of momentum equation, Eq. (7), is primarily due to $\langle u_i v \rangle_0$ at high Reynolds numbers, which is partially resolved. In terms of the average flow, $\overline{\langle u_i v \rangle_0} = \int_0^1 \overline{u_i^0 v^0} dy$ represents the turbulent enhancement of the skin-friction coefficient relative to a baseline laminar flow (Elnahhas & Johnson, 2022). Similarly, the fluxes $\langle u_i u_j \rangle_{0;1}$ in Eqs. (6) and (7) are partially resolved.

To understand how much of the Reynolds stresses may be directly resolved in the two-dimensional instantaneous wall-normal integral field, a triple decomposition for the velocity field is defined for and field, f, as

$$f = \overline{f} + f^0 = \overline{f} + \langle f \rangle_0 + f^{00}. \tag{10}$$

where $\overline{f}$ is the Reynolds average The turbulent fluctuations resolved by the two-dimensional integral field is $\langle f^0 \rangle_0$ and the unresolved remained is f^{00}. Thus, any covariance maybe decomposed into resolved and unresolved parts,

$$\overline{f^0 y^0}^{\,}_{0} = \overline{\langle f \rangle_0 \langle y \rangle_0} + \overline{f^{00} y^{00}}^{\,}_{0}. \tag{11}$$

The fraction of any covariance which is resolved in the two-dimensional representation is defined as,

$$T_{fy} = \frac{\overline{\langle f \rangle_0 \langle y \rangle_0}}{\overline{f^0 y^0}^{\,}_{0}}. \tag{12}$$

The results of the resolved percentages of the Reynolds stress components by the wall-normal integration for each flow case are arranged in the 'All Scales' section of Table 2. When compared at the same Re_t, the half-channel and full-channel flows produce very similar results. For the Reynolds numbers shown, roughly 40% – 50% of the Reynolds shear stress integral (the main sink term in Eq. (7)) is resolved by the 2D velocity integral field. The percent resolution, T_{uv}, decreases slowly with increasing Reynolds number.

The resolution of the diagonal (kinetic energy) components of the Reynolds stress tensor is significantly lower than the shear stress, especially for the spanwise fluctuations, T_{ww}. This indicates that the resolved velocity integral field is more efficient at capturing more active motions of turbulence (i.e., those which contribute more to the momentum transport across the layer). The percent resolution of spanwise and wall-normal kinetic energy decreases with increasing Reynolds number, but the streamwise kinetic energy remains at a nearly constant at 33% resolution across the Reynolds numbers investigated.

The 'Large Scales' section of Table 2 recalculates the resolution fractions using only the largest scales, here defined by $k_x h < 1$ (see, e.g., Kim & Adrian (1999), Monty *et al.* (2009)). The large-scale contributions to the Reynolds shear stress integral is & 60% resolved, showing that the 2D velocity integral field is more efficient at resolving larger-scale motions. Furthermore, the fractional resolution grows with increasing Reynolds number, a reversal of the trend observed when all scale of motion are included. The fractional resolution of streamwise and wall-normal kinetic energy is likewise higher when only the large scales are included, though the spanwise kinetic energy resolution is not higher. The streamwise kinetic energy resolution for large scales also grows with increasing Reynolds number, while the other two components remain relatively constant. There are no significant differences between half-channel and full-channel turbulent flows. Based on averaging over 20 flow-through times, the statistical uncertainties of these results are estimated to be on the order of 0.1% for the $Re_t = 180$ and 395 cases. The uncertainty is larger (up to 2%) for the JHTDB $Re_t = 1000$ case because only one flow through time is available.

To further investigate the scale-wise resolution of wall-normal integrals, the resolution fraction may be defined on a scale-by-scale basis as

$$T_{fy}(k_x) = \frac{\overline{\langle \hat{f} \rangle_0 \langle \hat{y} \rangle_0}}{\overline{\langle \hat{f} \hat{y} \rangle_0}}; \tag{13}$$

where the $\hat{(\cdot)}$ denotes a Fourier transform in the streamwise direction and $(\cdot)^*$ denotes the complex conjugate. This may be thought of as a transfer function for the wall-normal integral operator. The transfer functions for the TKE (left) and Reynolds shear stress (right) are plotted for all flow cases in Figure 2. As reflected in Table 2, larger scales (smaller wavenumbers) are more resolved than smaller scales, as may be expected. If anything, $\hat{T}_{uu+vv+ww}$ and $\hat{T}_{uv}$ decrease relatively slowly with increasing wavenumber compared to expectations, e.g., k_x^{-1} based on a naive interpretation of wall-normal integration as an anti-derivative in the streamwise direction. At larger scales, the percent resolution increases with increasing Reynolds number, but this trend reverses for small scales. This reversal explains the opposite trends seen in Table

Table 2. Percentage of the Reynolds stress component integrals resolved by instantaneous wall-normal integrals. The last column in each region of the table reports the resolved turbulent kinetic energy (TKE).

	All Scales					Large Scales				
Case	T_{uu}	T_{vv}	T_{ww}	T_{uv}	$T_{uu+vv+ww}$	T_{uu}	T_{vv}	T_{ww}	T_{uv}	$T_{uu+vv+ww}$
180hc	34%	39%	16%	52%	31%	48%	48%	12%	61%	45%
395hc	34%	31%	13%	45%	28%	58%	46%	13%	64%	54%
180fc	33%	40%	16%	51%	30%	44%	46%	13%	58%	42%
395fc	31%	32%	13%	45%	27%	52%	46%	13%	62%	48%
1000fc	33%	26%	11%	42%	26%	59%	47%	14%	66%	55%

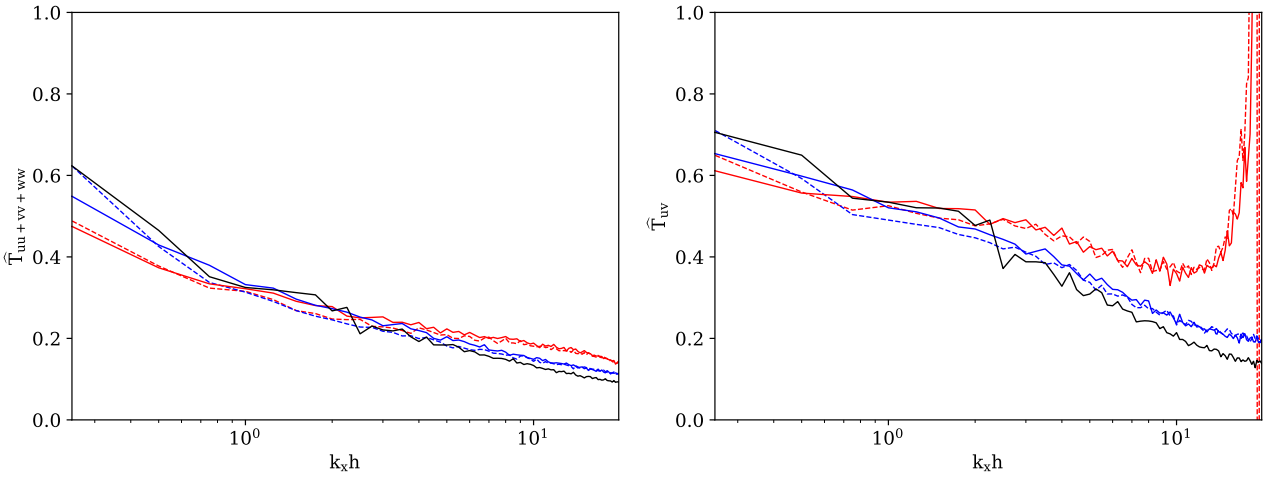

Figure 2. As a function of streamwise wavenumber, the percent resolution of Reynolds stresses: TKE (left), shear stress (right).

2. The transfer functions in Figure 2 are very similar for full-channel and half-channel flows when compared at the same Reynolds number. Note that $\widehat{T}_{uv}$ diverges for $Re_t = 180$ cases at $k_x \gtrsim 20$ because the smaller scale motions becomes close to locally isotropic, causing the denominator in Eq. (13) to approach zero. This effect is also seen for the higher Reynolds number cases at higher wavenumbers.

CONDITIONAL AVERAGES

While the previous section quantifies the extent to which a two-dimensional velocity integral field resolves turbulent fluctuations, there inevitably remains unresolved flow physics requiring approximate models to close Eqs. (6) and (7). To lay the groundwork for developing closure approximations, this section explores the statistics of unclosed terms as well as the resolved 2D velocity integral fields, $\hbar u_i i_0$ and $\hbar u_i i_1$. Note that the first moment of the mass conservation equation yields an equation for $\hbar v i_0$ in terms of the divergence of $\hbar u_i i_1$.

Figure 3 illustrates the standardized probability density function (PDF) of the zeroth and first streamwise velocity moments for the half-channel flow DNS results. The mean, standard deviation, skewness, and kurtosis values are shown in Table 3. The mean zeroth moment is the flow rate (normalized using friction velocity and half-channel height). The mean first moment is larger than the zero moment because the first moment puts more weight to the higher velocity regions further from the no-slip wall. The mean value of both moments grow as Reynolds number increases because of the normalization

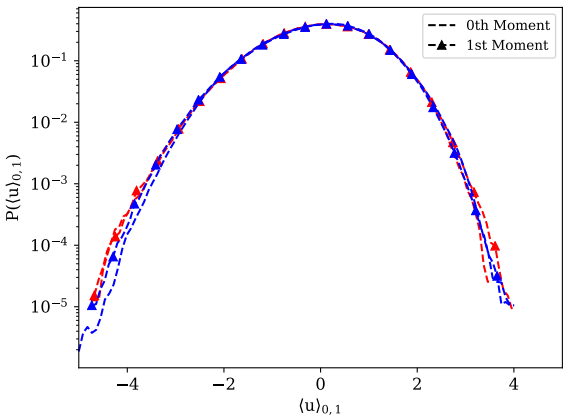

Figure 3. Standardized PDF of the velocity moments. The color code and line types of these plots correspond to Table 1. The plots with no marker correspond to the zeroth moment and the plots with triangle markers signify the first moment.

with respect to the friction velocity. The zeroth and first moment integrals fluctuate significantly, as visually shown in Figure 1. Interestingly, the standard deviation for the first moment is slightly smaller than the zeroth moment, the opposite trend as the mean. The skewness and kurtosis values indicate that the fluctuations are fairly close to Gaussian, see also Figure 3.

Next, to develop understanding of how unclosed terms can be approximated in terms of known variables, condi-

Table 3. Single-point statistics for the zeroth and first moments of streamwise velocity, Eq.(4).

Re_t	180		395	
$\langle u \rangle_{0;1}$	$\langle u \rangle_0$	$\langle u \rangle_1$	$\langle u \rangle_0$	$\langle u \rangle_1$
Mean	15.75	17.31	17.61	19.03
Std. Dev.	0.90	0.80	0.87	0.81
Skewness	-0.22	-0.20	-0.17	-0.26
Kurtosis	2.90	2.96	2.86	2.93

tional averages of these terms are calculated conditioned on the zeroth and/or first velocity moments. Figure 4 illustrates the conditionally-averaged wall shear stress in the streamwise direction (left) and the zeroth moment of the unresolved Reynolds shear stress (right), see Eq. (6) and (7), respectively. In this figure, the averages are conditioned on either the zeroth or first moment of the velocity profile.

Of course, the wall-shear stress will increase with respect to both of the velocity moments due to higher velocity gradient effects. All four curves are strikingly linear. The slope for the zeroth moment is higher than the first moment because the first moment places a higher weight on the velocity further from the wall, which is less influential in setting the velocity gradient at the wall. It is also noted that a positive shift occurs as Re_t increases, which is simply due to the increasing average velocities when normalized on the friction velocity, Table 3.

The conditional average of the unresolved turbulent mixing is more interesting. For both Reynolds numbers, it does not have a strong negative or positive trend with the zeroth moment. It does, however, strongly increase with increasing first moment. This trend may be explained by the fact that the first moment is more influential in setting the distribution of the local shear and the potential presence of local inflection points that may accelerate the production of unresolved turbulence.

Figure 5 plots the conditionally-averaged wall shear stress (left) and the zeroth moment of the unresolved Reynolds shear stress (right) conditioned simultaneously on both velocity moments. These conditional averages are based on the $Re_t = 180$ half-channel (180hc) case. The behavior of these conditional averages generally coincide with the results in Figure 4 in the sense that the wall shear stress increases with the velocity moments. A richer view emerges, however. For example, the conditionally-averaged wall stress decreases with increasing first moment if the zeroth moment is held fixed. The explanation for this trend is as follows. For a fixed flow rate, increasing the first moment increases the velocity further from the wall while slowing down the fluid near the wall. The result is a reshaping of the local velocity profile so as to decrease its slope at the wall and hence its wall shear stress. Interestingly, as in Figure 4, the strong positive correlation between the zeroth and first moment fluctuations recovers a positive slope when the stress is only conditioned on the first moment.

The opposite trend may be observed in the right panel of Figure 5. For a fixed zeroth moment, an increase in the first moment increases the conditional average of the unresolved Reynolds shear stress integral. To explain this, consider that the increase of the first moment at fixed flow rate moves the local shear away from the wall. Given that turbulent production is proportional to the shear, the local production of unresolved turbulence is more likely further from the wall. The wall damping effect (wall-blocking) is thus reduced allowing for more vigorous unresolved turbulent mixing of momentum.

CONCLUSIONS

In this work, the dynamical equations for instantaneous wall-normal integrals of the velocity field are established for a half-channel configuration. The integral equations are developed from the Navier-Stokes equation for the zeroth and first wall-normal moment. Direct numerical simulations are employed to study key sink terms in the moment equations, namely, the wall shear stress and the integral of the Reynolds shear stress across the half-channel. The results show that nearly 50% of the Reynolds shear stress is resolved by the two-dimensional instantaneous integral representation. This fraction decreases with increasing Reynolds number, however, because the introduction of a wider range of small-scale motions increases the proportion of turbulent fluctuations that are filtered out by the wall-normal integration procedure. On the other hand, the fraction of resolved Reynolds shear stress integral increases to & 60% when considering only contributions from $k_x h < 1$. More importantly, the resolution fraction for these large-scale motions increases with increasing Reynolds number. DNS of half-channel and full-channel configurations lead to very similar results, but the extension and application of the framework to turbulent boundary layers is an important future topic. Finally, conditional averages of the unresolved part of the sink terms show a strong dependence on the local value of the resolved terms, providing a path forward to constructing predictive models.

ACKNOWLEDGEMENT

TR was supported by the Department of Defense (DoD) through the National Defense Science & Engineering Graduate (NDSEG) Fellowship Program. PJ was supported by the National Science Foundation under CAREER award No. 2340121.

REFERENCES

Balakumar, B. J. & Adrian, R. J. 2007 Large- and very-large-scale motions in channel and boundary-layer flows. *Phil. Trans. Royal Soc. A* **365** (1852), 665–681.

Elnahhas, Ahmed & Johnson, Perry L 2022 On the enhancement of boundary layer skin friction by turbulence: an angular momentum approach. *Journal of Fluid Mechanics* **940**, A36.

Goc, K., Bose, S. & Moin, P. 2020 Wall-modeled large eddy simulation of an aircraft in landing configuration. In *AIAA Aviation 2020 Forum*, p. 3002.

Graham, J., Kanov, K., Yang, X. I. A., Lee, M., Malaya, N., Lalescu, C. C., Burns, R., Eyink, G., Szalay, A., Moser, R. D. & Meneveau, C. 2016 A web services accessible database of turbulent channel flow and its use for testing a new integral wall model for les. *Journal of Turbulence* **17** (2), 181–215.

Guala, M., Hommema, S. E. & Adrian, R. J. 2006 Large-scale and very-large-scale motions in turbulent pipe flow. *Journal of Fluid Mechanics* **554**, 521–542.

Harun, Z., Monty, J. P., Mathis, R. & Marusic, I. 2013 Pressure gradient effects on the large-scale structure of turbulent boundary layers. *Journal of Fluid Mechanics* **715**, 477–498.

Hutchins, N. & Marusic, I. 2007 Evidence of very long meandering features in the logarithmic region of turbulent boundary layers. *Journal of Fluid Mechanics* **579**, 1–28.

Jimenez, J. 1998 The largest scales of turbulent wall flow. *Center for Turbulence Research Annual Research Briefs* pp. 137–153.